Beyond Shape Engineering of TiO2 Nanoparticles: Post-Synthesis Treatment Dependence of Surface Hydration, Hydroxylation, Lewis Acidity and Photocatalytic Activity of TiO2 Anatase Nanoparticles with Dominant 001 or 101 Facets

Supporting Information

Beyond Shape Engineering of TiO_2 Nanoparticles: Post-Synthesis Treatment Dependence of Surface Hydration, Hydroxylation, Lewis Acidity and Photocatalytic Activity of TiO_2 Anatase Nanoparticles with Dominant {001} or {101} Facets

Lorenzo Mino,[a*+] Francesco Pellegrino,[a+] Steffi Rades,[b] Jörg Radnik,[b] Vasile-Dan Hodoroaba,[b] Giuseppe Spoto,[a] Valter Maurino,[a] Gianmario Martra[a]

[a]Department of Chemistry and NIS Centre, University of Torino, via Giuria 7, 10125 Torino, Italy
[b]Federal Institute for Materials Research and Testing (BAM), 12205 Berlin, Germany

[+]These authors contributed equally to this work

Corresponding Author
*E-mail: lorenzo.mino@unito.it

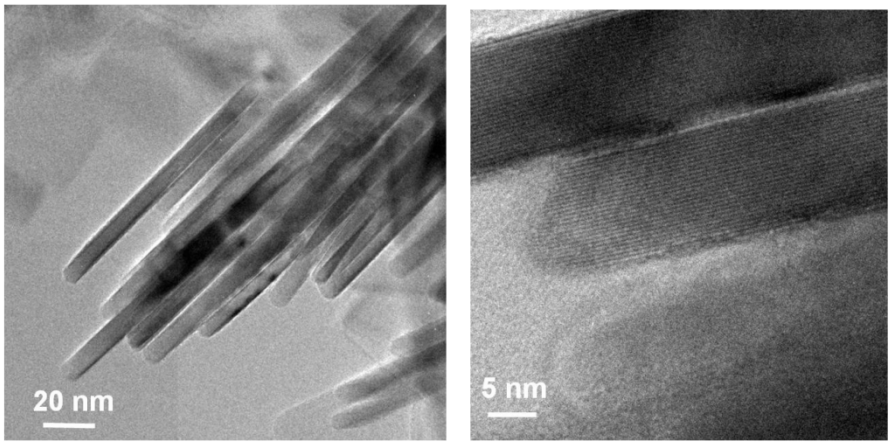

Figure S1. HR-TEM images of TiO_2 n-sh_NaOH.

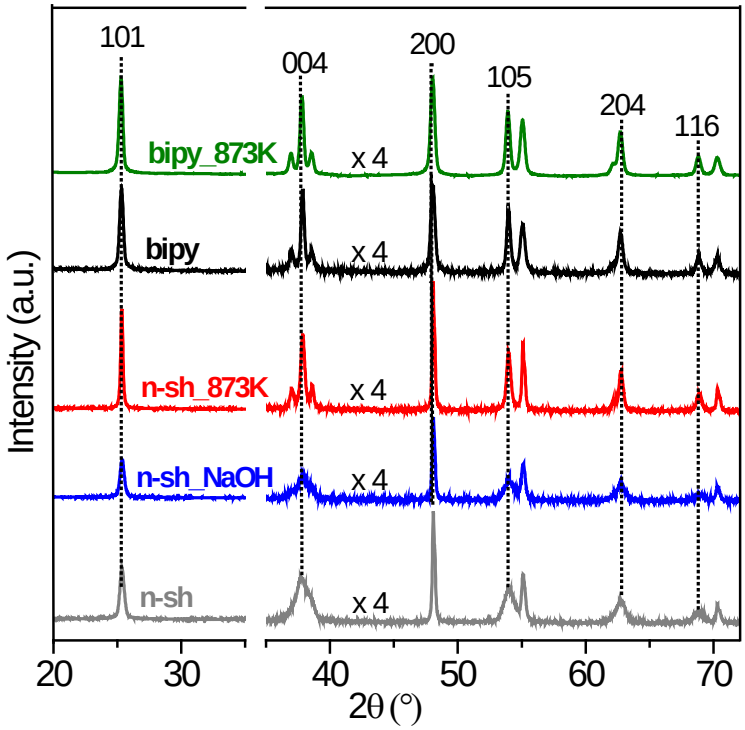

Figure S2. XRD patterns of the pristine and treated forms of TiO_2 nano-sheets and TiO_2 bipy nanoparticles. All signals correspond to anatase TiO_2 reflections, according to ICDD PDF 00-021-1272. The main peaks are labeled, including those considered for the Scherrer analysis. The ordinate scale in the right part of the patterns, after the break in the abscissa axis, has been magnified 4 times.

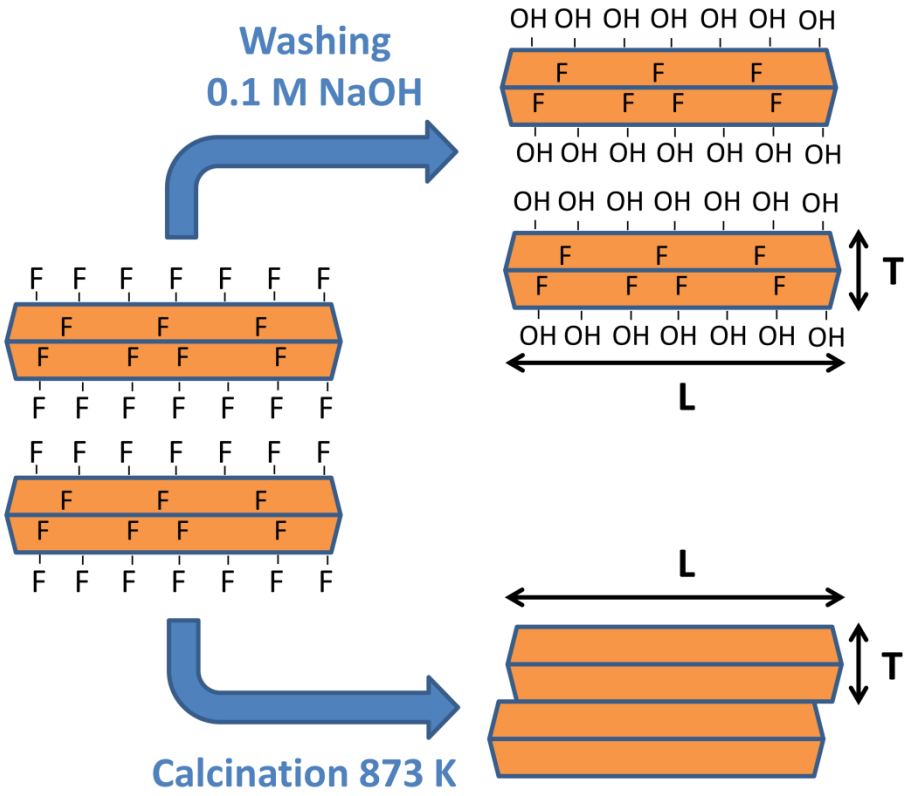

Figure S3. Schematic representation of the effect of the treatments performed to remove fluorides from the as-synthesized TiO_2 n-sh. T and L are the thickness and length of nanoparticles reported in Table 1, as determined by electron microscopy.

Calculation of expected specific surface area and percentage of exposed {001} surfaces

To calculate the expected specific surface area (SSA_e) and percentage of exposed {001} surfaces, we built a geometric model using the electron microscopy dimensional data (see Table 1 in the main text). The formulas employed in the calculations are reported in the following:

$$l_{101} = \frac{T}{2sin\alpha}$$

$$l_{001} = L - 2l_{101}cos\alpha$$

$$A_{tot} = 2{l_{001}}^2 + 2\left[\frac{(4L + 4l_{001}) * l_{101}}{2}\right]$$

$$V_{tot} = \frac{1}{3}\frac{T}{2}\left(L^2 + {l_{001}}^2 + \sqrt{L * l_{001}}\right) * 2$$

$$SSA_e = A_{tot} * \frac{1}{\rho * V_{tot}}$$

where ρ is the TiO_2 density and the other symbols are reported in Figure S4.

The result of the calculation is SSA_e = 66 m^2/g for the TiO_2 n-sh sample.

For the TiO_2 n-sh_873K sample we considered a model in which pairs of NPs share one {001} facet (see Figure S3) and therefore we employed a modified formula to calculate the total exposed surface area for a pair of sintered NPs:

$$A_{tot} = 2{l_{001}}^2 + 4\left[\frac{(4L + 4l_{001}) * l_{101}}{2}\right]$$

In this case the result of the calculation is SSA_e = 41 m^2/g. The trend is in excellent agreement with the experimental SSA_{BET} data (see Table 1 in the main text) and confirms the XRD data which suggest that the primary NPs could have sintered in pairs.

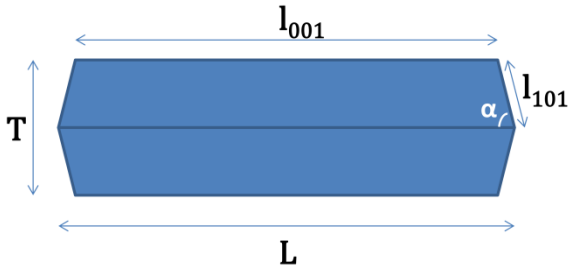

Figure S4. Schematic representation of the geometrical model employed to calculate the expected specific surface area (SSA_e) and percentage of exposed {001} surfaces.

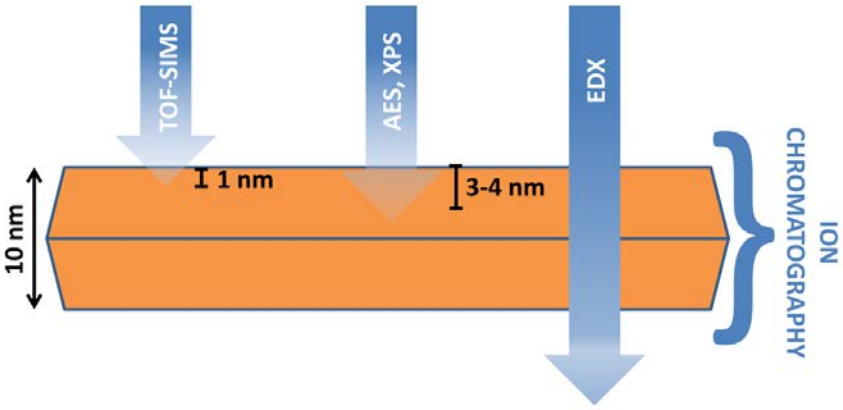

Figure S5. Schematic representation of a TiO_2 n-sh showing the probing depth for the different analytical techniques employed to identify the presence of fluorides.

SEM/EDX

Energy dispersive X-ray spectroscopy has been applied on microscopic (500 µm x 500 µm) sample areas defined on scanning electron micrographs. The information depth associated to the X-ray signals reaches typically the (sub-)micrometer range. F K X-ray line was detected only in the samples n-sh and n-sh_NaOH at a comparable intensity level. Similar to the AES analysis, the other two samples n-sh_873K and bipy have provided only 'noise' signals. The limit of detections of electron probe microanalysis are in the range of 0.1 mass-%. The quantification of the X-ray signals detected cannot be applied accurately due to the strong sample morphology at the (sub-) µm scale.

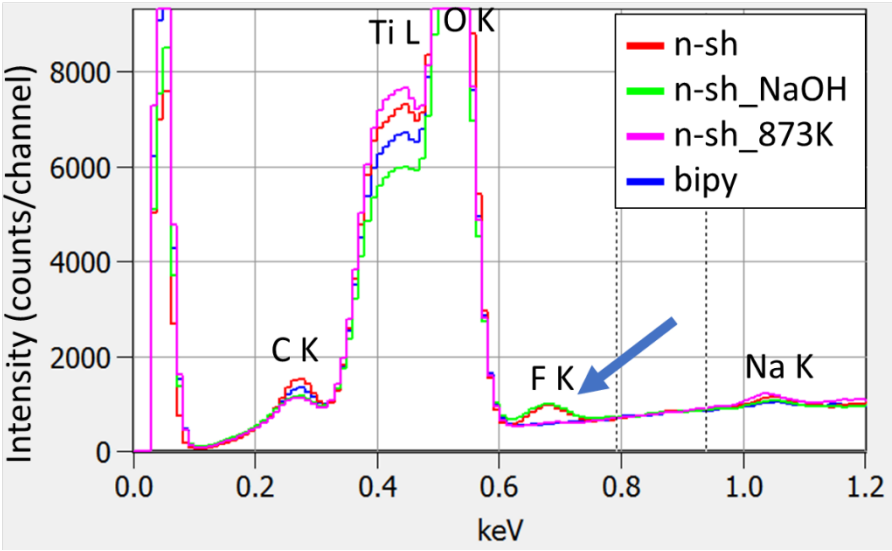

Figure S6. 10 kV EDX spectra of the samples n-sh, n-sh_NaOH, n-sh_873K and bipy (measured over a 500 µm by 500 µm area of the nanoparticulate material prepared on silicon wafer as a substrate). The spectra have been normalized to the background signal between 0.79 and 0.95 keV.

Auger electron spectroscopy

Auger electron spectroscopy (AES) has been applied in order to take advantage of both excellent lateral resolution of the Auger probe (in the range of 10 nm) as well as of the information depth (about 3-4 nm). Hence, areas significantly smaller than that of individual TiO_2 nano-sheets could be analyzed. Figure S7 shows two examples of AES analysis where individual nano-sheets of the samples n-sh and n-sh_873K have been inspected. Note the distinct Auger signal detected on the n-sh sample. Under the same analysis conditions, the calcinated sample does not show any F KLL signal. It should be noticed that the limits of detection of AES are in the range of sub-percent, so that any presence of fluorine at (ultra-)trace level cannot be detected.

In general, a level of fluorine similar to that in the sample n-sh has been detected in n-sh_NaOH sample. The quantification of the Auger signals into absolute concentrations constitutes a challenging task. Particularly for the TiO_2 nano-sheets as in the present study, the strong sample morphology at the nanometer scale makes the reliability of quantification very poor, so that direct comparison of spectra taken under same experimental conditions remains a means for reliable semi-quantitative evaluation.[1] Further, the 'noise' level of fluorine as detected for the n-sh_873K sample, indicating the removal of fluorine from the 3-4 nm depth sampled by AES, has been confirmed by measurements on the bipy sample, also showing no F KLL signal.

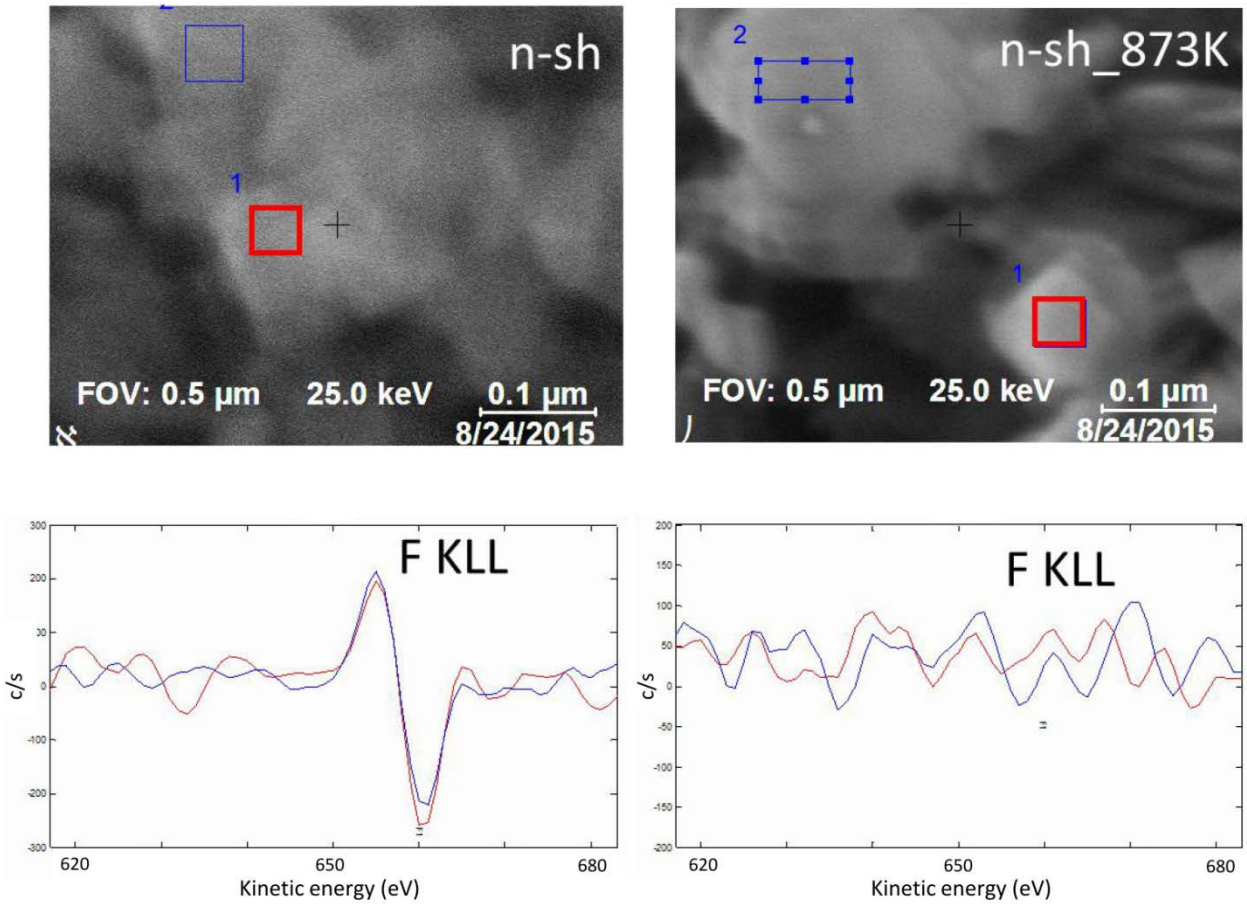

Figure S7. 25 kV Auger electron spectra of the samples n-sh and n-sh_873K (measured over a 400 nm by 400 nm area on two nano-sheets, respectively). Due to the poor (typically) signal-to-background Auger peaks, the Auger spectra have been differentiated.

ToF-SIMS

The highest elemental sensitivity of all analytical methods employed in the present study is offered by ToF-SIMS (time-of-flight secondary ion mass spectrometry). Elements present in the outermost 1 nm at the sample surface can be detected at the ppm (sometimes even ppb) level. The strong matrix effects are well-known to hamper seriously an accurate SIMS quantification. Similar to the other analytical techniques, in order to be able to compare the results obtained for different samples at least in a semi-quantitative manner, normalization to a signal of an internal element and/or relation to reference materials measured under the same conditions are necessary. Figure S8 shows the peak of the negative fluorine ion as detected in the samples n-sh and n-sh_873K after normalization to the TiO_2 signal from each ToF-SIMS spectrum acquired at different 9 locations on each sample. Note the clear difference by a factor of about 20 between the F intensity corresponding to sample n-sh and the n-sh_873K sample. As resumed in Table 2 of the main text, sample n-sh_NaOH provides a significantly lower signal of F^-. Further, the low level of F^- found in sample n-sh_NaOH is comparable to the level of F^- detected in the sample bipy, but also in the

fluorine-free silicon substrate. Hence, the conclusion drawn is that this fluorine level is sample independent and shows the limits of detection of the ToF-SIMS instrument used in the conditions given as a rest level. Note that all the other analytical techniques IC, EDX and AES could not detect presence of fluorine in both samples n-sh_873K and the reference bipy.
The reproducibility of the ToF-SIMS results has been confirmed by measurements carried out at different times and by preparing the samples on alternative substrates (e.g. silver foils).

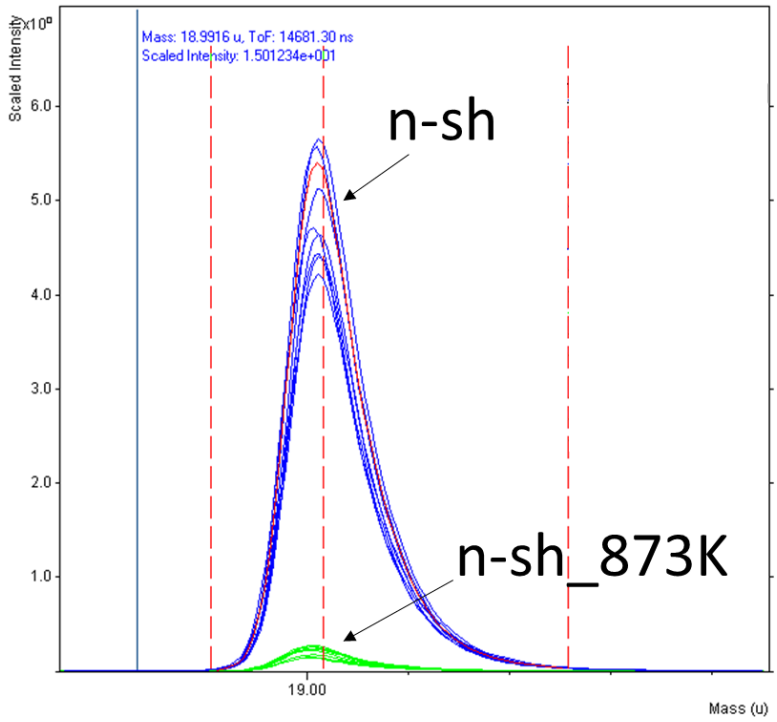

Figure S8. Fluorine signal in the ToF-SIMS spectra of the samples n-sh (blue) and n-sh_873K (green) measured over a 100 µm x 100 µm area at nine different locations on each sample prepared on a silicon substrate. For comparison purpose, the F^- signal (recorded in a window around 18.9916 a.m.u.) has been normalized to the TiO_2 signal at 79.9374 a.m.u.

XPS

For F1s two states were observed (Figure S7): inorganic fluoride with an electron binding energy of 684 eV and small amounts of organic fluorine with a binding energy of 689 eV. The organic fluorine probably comes from a small contamination due to the use of a Teflon lined stainless steel reactor during the sample synthesis. The treatments (washing with NaOH or calcination at 873 K) influenced mainly the inorganic F. In the case of n-sh_873K and bipy samples, XPS is working at its limits of detection, roughly corresponding to 0.1 at.-%.

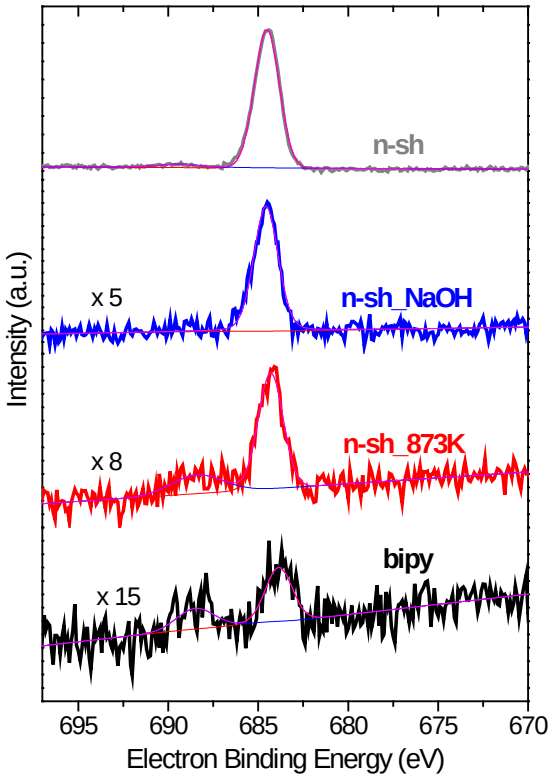

Figure S9. F1s XPS spectra of the TiO_2 samples and related components of the spectral deconvolution.

In the Ti2p XPS spectra reported in Figure S10 we can identify three main components ascribed to $Ti^{4+}2p_{1/2}$ at 464.5 eV, to $Ti^{4+}2p_{3/2}$ at 459.9 eV and to the main peak of $Ti^{4+}2p_{3/2}$ at 458.8 eV.[2] The binding energy of 459.9 eV is significantly higher than the ones of pure TiO_2 and can be explained by the influence of the F^- anions.[3] The intensity ratio between this Ti^{4+} component and the main $Ti^{4+}2p_{3/2}$ signal decreased from 0.3 for TiO_2 n-sh to *ca.* 0.1 for the other samples, in agreement with the evolution of the electronic properties highlighted by UV-Vis-NIR-MIR spectroscopy and with the progressive decrease of F^- content (see Table 2 in the main text). The small shoulder at 456.8 eV suggests that a contribution of Ti^{3+} to the Ti2p signal can be also present, especially for the TiO_2 n-sh sample.[4]

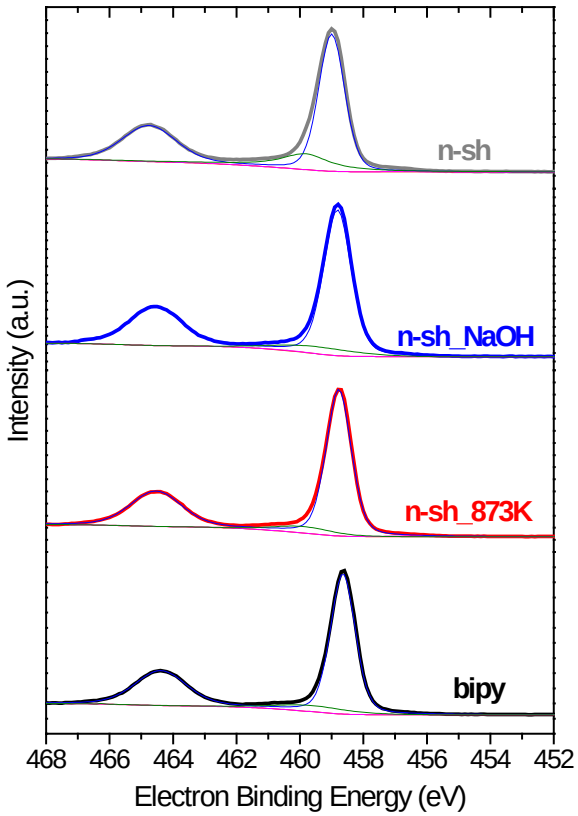

Figure S10. Ti2p XPS spectra of the TiO_2 samples and related components of the spectral deconvolution.

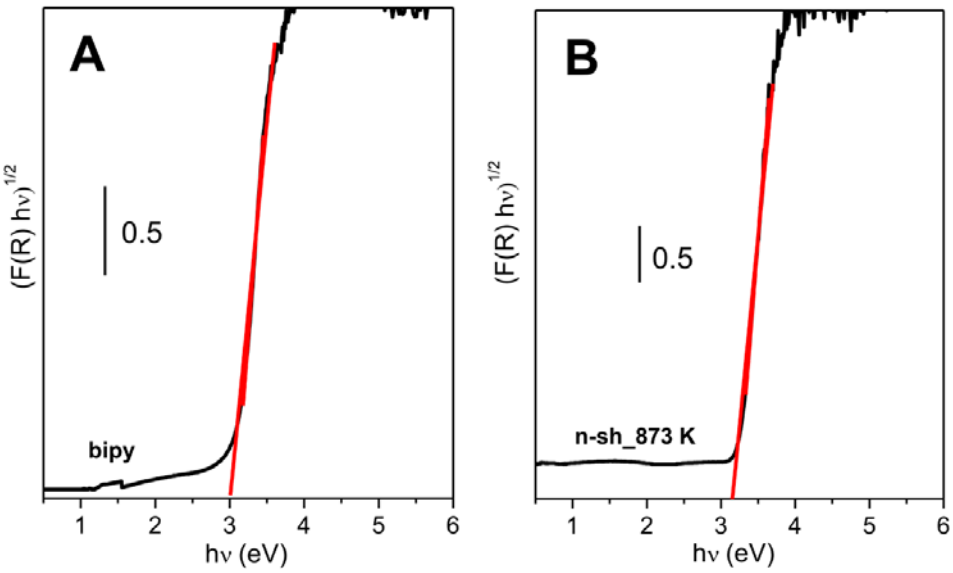

Figure S11. Tauc plot for the bipy (A) and n-sh_873 (B) samples. The red lines represent the linear fit to the function $(F(R)\ h\nu)^{1/2} = A\ h\nu + B$, where for bipy A = 5.52337 ± 0.7206 and B = -17.08975 ± 0.23877, while for n-sh_873 A = 8.31729 ± 0.09926 and B = -27.10771 ± 0.34605.

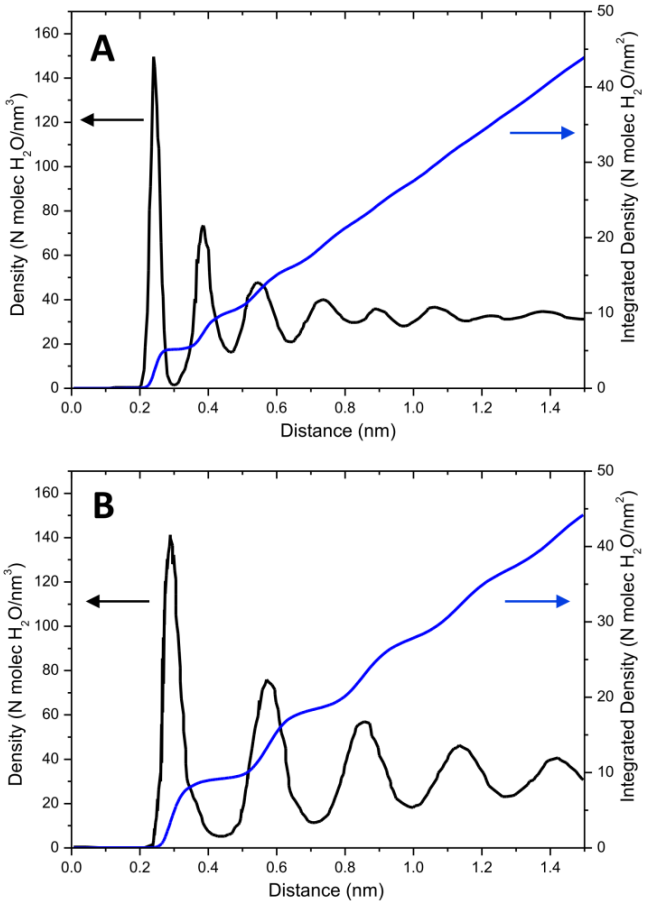

Figure S12. Water density profile and corresponding integration in the direction normal to the (101) (panel A) and (001) (panel B) TiO_2 anatase surfaces. The molecular dynamics simulation data have been extracted from Figure 3b of ref. [5]

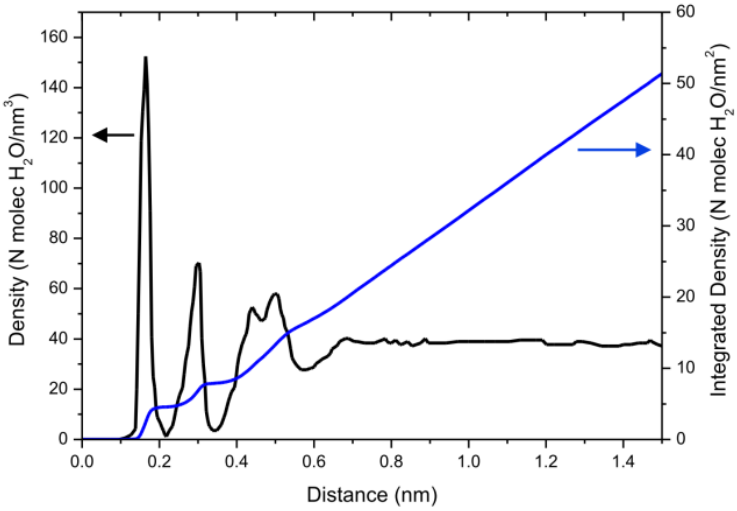

Figure S13. Water density profile and corresponding integration in the direction normal to the (101) TiO_2 anatase surface. The molecular dynamics simulation data have been extracted from Figure 2 of ref. [6]

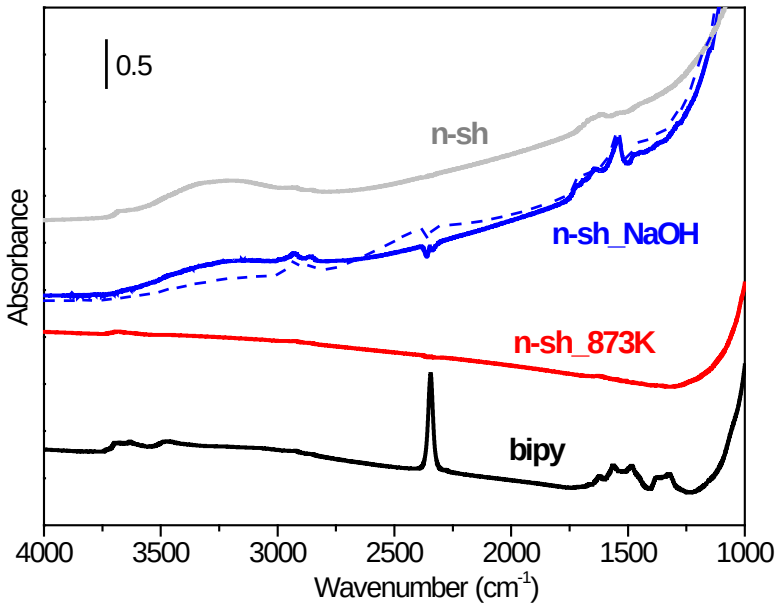

Figure S14. FT-IR spectra of the samples after outgassing for 1 hour at r.t. The spectrum of the TiO_2 n-sh_NaOH contacted with D_2O and outgassed for 1 hour at r.t., employed to remove the contributions due to bare TiO_2, is also reported as a dashed curve.

Table S1. Assignment of the main IR spectral features of CO adsorbed on TiO_2 NPs (Figure 7).[7-8]

Band position (cm^{-1})	**Assignment**
2180-2178	^{12}CO on {101} surfaces
2165-2163	^{12}CO on {100} surfaces
2156-2155	^{12}CO on {001} surfaces
2139-2138	Liquid-like CO
2127-2126	^{13}CO on {101} surfaces

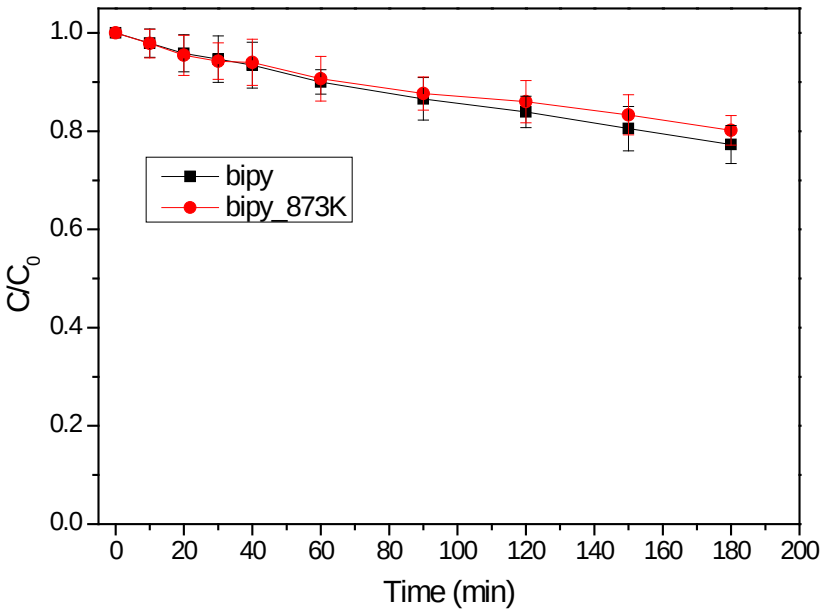

Figure S15. Phenol photodegradation curves for TiO_2 bipy and TiO_2 bipy_873K samples.

References

(1) Ortel, E.; Hausler, I.; Osterle, W.; Narbey, S.; Oswald, F.; Andersen, I. H.; Holzweber, M.; Unger, W. E. S.; Hodoroaba, V.-D. In-Depth Structural and Chemical Characterization of Engineered TiO_2 Films. *Surf. Interface Anal.* **2016,** *48*, 664-669.
(2) Bharti, B.; Kumar, S.; Lee, H. N.; Kumar, R. Formation of Oxygen Vacancies and Ti^{3+} State in TiO_2 Thin Film and Enhanced Optical Properties by Air Plasma Treatment. *Sci Rep* **2016,** *6*, 12.
(3) Jangir, M.; Jain, A.; Yamaguchi, S.; Ichikawa, T.; Lal, C.; Jain, I. P. Catalytic Effect of TiF_4 in Improving Hydrogen Storage Properties of MgH_2 *Int. J. Hydrogen Energy* **2016,** *41*, 14178-14183.
(4) Radnik, J.; Mohr, C.; Claus, P. On the Origin of Binding Energy Shifts of Core Levels of Supported Gold Nanoparticles and Dependence of Pretreatment and Material Synthesis **2003,** *5*, 172-177.
(5) Kavathekar, R. S.; Dev, P.; English, N. J.; MacElroy, J. M. D. Molecular Dynamics Study of Water in Contact with the TiO_2 Rutile-110, 100, 101, 001 and Anatase-101, 001 Surface. *Mol. Phys.* **2011,** *109*, 1649-1656.
(6) English, N. J. Diffusivity and Mobility of Adsorbed Water Layers at TiO_2 Rutile and Anatase Interfaces. *Crystals* **2016,** *6*, 1-7.
(7) Mino, L.; Spoto, G.; Bordiga, S.; Zecchina, A. Particles Morphology and Surface Properties as Investigated by HRTEM, FTIR, and Periodic DFT Calculations: From Pyrogenic TiO_2 (P25) to Nanoanatase. *J. Phys. Chem. C* **2012,** *116*, 17008-17018.
(8) Deiana, C.; Minella, M.; Tabacchi, G.; Maurino, V.; Fois, E.; Martra, G. Shape-Controlled TiO_2 Nanoparticles and TiO_2 P25 Interacting with CO and H_2O_2 Molecular Probes: A Synergic Approach for Surface Structure Recognition and Physico-Chemical Understanding. *Phys. Chem. Chem. Phys* **2013,** *15*, 307-15.